Faraday effect in hybrid magneto-plasmonic photonic crystals

B. Caballero,[1,2] **A. García-Martín,**[1,3] **and J. C. Cuevas**[2,4]

[1]*IMM-Instituto de Microelectrónica de Madrid (CNM-CSIC), Isaac Newton 8, PTM, Tres Cantos, E-28760 Madrid, Spain*
[2]*Departamento de Física Teórica de la Materia Condensada and Condensed Matter Physics Center (IFIMAC), Universidad Autónoma de Madrid, E-28049 Madrid, Spain*
[3]*a.garcia.martin@csic.es*
[4]*juancarlos.cuevas@uam.es*

Abstract: We present a theoretical study of the Faraday effect in hybrid magneto-plasmonic crystals that consist of Au-Co-Au perforated membranes with a periodic array of sub-wavelength holes. We show that in these hybrid systems the interplay between the extraordinary optical transmission and the magneto-optical activity leads to a resonant enhancement of the Faraday rotation, as compared to purely ferromagnetic membranes. In particular, we determine the geometrical parameters for which this enhancement is optimized and show that the inclusion of a noble metal like Au dramatically increases the Faraday rotation over a broad bandwidth. Moreover, we show that the analysis of the Faraday rotation in these periodically perforated membranes provides a further insight into the origin of the extraordinary optical transmission.

References and links

1. S. A. Maier, *Plasmonics: Fundamentals and Applications* (Springer, 2007).
2. J. A. Schuller, E. S. Barnard, W. Cai, Y. C. Jun, J. S. White, and M. L. Brongersma, "Plasmonics for extreme light concentration and manipulation," Nat. Mater. **9**, 193–204 (2010).
3. G. Armelles, A. Cebollada, A. García-Martín, J. M. García-Martín, M. U. González, J. B. González-Díaz, E. Ferreiro-Vila, and J. F. Torrado, "Magnetoplasmonic nanostructures: systems supporting both plasmonic and magnetic properties," J. Opt. A: Pure Appl. Opt. **11**, 114023 (2009).
4. G. Armelles, A. Cebollada, A. García-Martín, and M. U. González, "Magnetoplasmonics: magnetoplasmonics: combining magnetic and plasmonic functionalities," Adv. Opt. Mater. **1**, 10 (2013).
5. V. Belotelov, L. Doskolovich, and A. Zvezdin, "Extraordinary magneto-optical effects and transmission through metal-dielectric plasmonic systems," Phys. Rev. Lett. **98**, 077401 (2007).
6. J. B. González-Díaz, B. Sepúlveda, A. García-Martín, and G. Armelles, "Cobalt dependence of the magneto-optical response in magnetoplasmonic nanodisks," Appl. Phys. Lett. **97**, 043114 (2010).
7. J. C. Banthí, D. Meneses-Rodríguez, F. García, M. U. González, A. García-Martín, A. Cebollada, and G. Armelles, "High magneto-optical activity and low optical losses in metal-dielectric Au/Co/Au-SiO(2) magnetoplasmonic nanodisks," Adv. Mater. **24**, OP36–41 (2012).
8. V. E. Kochergin, A. Yu. Toporov, and M. V. Valeiko, "Polariton enhancement of the Faraday magnetooptic effect," JETP Lett. **68**(5), 400-403 (1998).
9. J. Y. Chin, T. Steinle, T. Wehlus, D. Dregely, T. Weiss, V. I. Belotelov, B. Stritzker, and H. Giessen, "Nonreciprocal plasmonics enables giant enhancement of thin-film Faraday rotation," Nat. Commun. **4**, 1599 (2013).
10. A. N. Kuzmichev, L. E. Kreilkamp, M. Nur-E-Alam, E. Bezus, M. Vasiliev, I. A. Akimov, K. Alameh, M. Bayer, and V. I. Belotelov, "Tunable optical nanocavity of iron-garnet with a buried metal layer," Materials **8**, 3012-3023 (2015).

11. V. I. Belotelov, I. A. Akimov, M. Pohl, V. A. Kotov, S. Kasture, A. S. Vengurlekar, A. V. Gopal, D. R. Yakovlev, A. K. Zvezdin, and M. Bayer, "Enhanced magneto-optical effects in magnetoplasmonic crystals," Nat. Nanotech. **6**, 370–6 (2011).
12. L. E. Kreilkamp, V. I. Belotelov, J. Y. Chin, S. Neutzner, D. Dregely, T. Wehlus, I. A. Akimov, M. Bayer, B. Stritzker, and H. Giessen, "Waveguide-plasmon polaritons enhance transverse magneto-optical Kerr effect," Phys. Rev. X **3**, 041019 (2013).
13. M. Diwekar, V. Kamaev, J. Shi, and Z. V. Vardeny, "Optical and magneto-optical studies of two-dimensional metallodielectric photonic crystals on cobalt films," Appl. Phys. Lett. **84**, 3112 (2004).
14. G. Ctistis, E. Papaioannou, P. Patoka, J. Gutek, P. Fumagalli, and M. Giersig, "Optical and magnetic properties of hexagonal arrays of subwavelength holes in optically thin cobalt films," Nano Lett. **9**, 1–6 (2009).
15. E. T. Papaioannou, V. Kapaklis, M. Giersig, P. Fumagalli, A. García-Martín, E. Ferreiro-Vila, and G. Ctistis, "Magneto-optic enhancement and magnetic properties in Fe antidot films with hexagonal symmetry," Phys. Rev. B **81**, 054424 (2010).
16. J. F. Torrado, E. T. Papaioannou, G. Ctistis, P. Patoka, M. Giersig, G. Armelles, and A. García-Martín, "Plasmon induced modification of the transverse magneto-optical response in Fe antidot arrays," Phys. Status Solidi (RRL) **4**, 271–273 (2010).
17. J. F. Torrado, J. B. González-Díaz, G. Armelles, A. García-Martín, A. Altube, M. López-García, J. F. Galisteo-López, A. Blanco, and C. López, "Tunable magneto-photonic response of nickel nanostructures," Appl. Phys. Lett. **99**, 193109 (2011).
18. E. T. Papaioannou, V. Kapaklis, E. Melander, B. Hjörvarsson, S. D. Pappas, P. Patoka, M. Giersig, P. Fumagalli, A. García-Martín, and G. Ctistis, "Surface plasmons and magneto-optic activity in hexagonal Ni anti-dot arrays," Opt. Express **19**, 23867–23877 (2011).
19. E. Melander, E. Östman, J. Keller, J. Schmidt, E. T. Papaioannou, V. Kapaklis, U. B. Arnalds, B. Caballero, A. García-Martín, J. C. Cuevas, and B. Hjorvarsson, "Influence of the magnetic field on the plasmonic properties of transparent Ni anti-dot arrays," Appl. Phys. Lett. **101**, 063107 (2012).
20. H. Fang, B. Caballero, E. M. Akinoglu, E. T. Papaioannou, A. García-Martín, J. C. Cuevas, M. Giersig, and P. Fumagalli, "Observation of a hole-size-dependent energy shift of the surface-plasmon resonance in Ni antidot thin films," Appl. Phys. Lett. **106**, 153104 (2015).
21. V. I. Belotelov and A. K. Zvezdin, "Magnetooptics and extraordinary transmission of the perforated metallic films magnetized in polar geometry," J. Magn. Magn. Mater. **300**(1), e260-e263 (2006).
22. A. B. Khanikaev, A. V. Baryshev, A. A. Fedyanin, A. B. Granovsky, and M. Inoue, "Anomalous Faraday effect of a system with extraordinary optical transmittance," Opt. Express **15**, 6612–22 (2007).
23. T. W. Ebbesen, H. J. Lezec, H. F. Ghaemi, T. Thio, and P. A. Wolff, "Extraordinary optical transmission through sub-wavelength hole arrays," Nature **391**, 667–669 (1998).
24. F. J. Garcia-Vidal, T. W. Ebbesen, and L. Kuipers, "Light passing through subwavelength apertures," Rev. Mod. Phys. **82**, 729–787 (2010).
25. C. Clavero, K. Yang, J. R. Skuza, and R. A. Lukaszew, "Magnetic field modulation of intense surface plasmon polaritons," Opt. Express **18**, 7743–7752 (2010).
26. D. Meneses-Rodríguez, E. Ferreiro-Vila, P. Prieto, J. Anguita, M. U. González, J. M. García-Martín, A. Cebollada, A. García-Martín, and G. Armelles, "Probing the electromagnetic field distribution within a metallic nanodisk," Small **7**, 3317–3323 (2011).
27. J. F. Torrado, J. B. González-Díaz, A. García-Martín, and G. Armelles, "Unraveling the relationship between electromagnetic field intensity and the magnetic modulation of the wave vector of coupled surface plasmon polaritons," New J. Phys. **15**, 075025 (2013).
28. F. Przybilla, A. Degiron, J.-Y. Laluet, C. Genet, and T. W. Ebbesen, "Optical transmission in perforated noble and transition metal films," J. Opt. A: Pure Appl. Opt. **8**, 458–463 (2006).
29. A. Zvezdin and V. Kotov, *Modern Magnetooptics and Magnetooptical Materials* (IOP Publishing, 1997).
30. D. Whittaker and I. Culshaw, "Scattering-matrix treatment of patterned multilayer photonic structures," Phys. Rev. B **60**, 2610–2618 (1999).
31. B. Caballero, A. García-Martín, and J. C. Cuevas, "Generalized scattering-matrix approach for magneto-optics in periodically patterned multilayer systems," Phys. Rev. B **85**, 245103 (2012).
32. P. B. Johnson and R. W. Christy, "Optical constants of the noble metals," Phys. Rev. B **6**, 4370–4379 (1972).
33. E. Ferreiro-Vila, J. González-Díaz, R. Fermento, M. González, A. García-Martín, J. García-Martín, A. Cebollada, G. Armelles, D. Meneses-Rodríguez, and E. Sandoval, "Intertwined magneto-optical and plasmonic effects in Ag/Co/Ag layered structures," Phys. Rev. B **80**, 125132 (2009).
34. A. Krishnan, T. Thio, T. Kim, H. Lezec, T. Ebbesen, P. Wolff, J. Pendry, L. Martín-Moreno, and F. J. García-Vidal, "Evanescently coupled resonance in surface plasmon enhanced transmission," Opt. Commun. **200**, 1–7 (2001).
35. H. Raether, *Surface Plasmons on Smooth and Rough Surfaces and on Gratings* (Springer-Verlag, 1988).

1. Introduction

The ability of metals to sustain surface plasmon polaritons (SPPs) has been the key to find new ways to concentrate light to sub-wavelength volumes and to manipulate its propagation in integrated photonic devices [1, 2]. In the search for an active control of the light propagation in plasmonic structures, a lot of attention has been devoted to systems that incorporate ferromagnetic materials to take advantage of their magneto-optical properties. The idea of combining plasmonic systems with magneto-optically active materials has given rise to a new field known as *magneto-plasmonics* [3, 4]. In this field, one of the central ideas is to control the light propagation via the modification of the plasmon properties with an externally applied magnetic field. Conversely, the resonant excitation of plasmons and its consequent confinement of the electromagnetic field are used to enhance the magneto-optical response of the system. Following this idea, it has been shown that by hybridizing ferromagnetic materials with noble metals, often making use of periodic nanostructuration, different magneto-optical (MO) effects can be enhanced such as the polar MO Kerr effect [5–7], the Faraday effect [5, 8–10] or the transverse MO Kerr effect [11, 12], which makes hybrid magneto-plasmonic structures very attractive for technological applications.

In this work we present a comprehensive theoretical study of the Faraday effect in hybrid membranes with periodic arrays of sub-wavelength holes. The goal of this work is to show that the combination of noble and ferromagnetic metals in the context of magneto-plasmonic photonic crystals can lead to an enhancement of the Faraday effect. In recent years the MO response of ferromagnetic membranes has been extensively investigated for the reflected waves (Kerr effect) [13–20]. However, it is remarkable that Faraday effect for this kind of structures has not been studied in detail and only a few works in literature deal with transmission in ferromagnetic holey membranes [21]. Previous investigations of the MO properties of transmitted light were carried out for other system configurations, usually nanostructures where the MO active material was either a continuous layer [5, 9] or the material filling the holes [22]. Moreover, to the best of our knowledge, there are no studies of hybrid membranes (including noble and ferromagnetic metals) with periodic arrays of sub-wavelength holes. The propagation of electromagnetic waves in the visible range through metal membranes of sub-wavelength holes is governed by the so-called *extraordinary optical transmission*. This phenomenon was discovered by Ebbessen and coworkers [23] and it has been explained in terms of the resonant excitation of SPPs in the interfaces between the metallic membranes and the surrounding dielectrics [24]. In this work we present a systematic theoretical study of the Faraday effect in hybrid Au-Co-Au perforated membranes with two-dimensional periodic arrays of sub-wavelength holes. We show that the combination of noble and ferromagnetic metals leads to an improvement of the performance of these perforated membranes as Faraday rotators. In particular, we show that the excitation of the surface plasmons responsible for the occurrence of the extraordinary optical transmission gives rise to an enhancement in the Faraday rotation that coexists with the relatively high transmission. Moreover, as the MO response in hybrid nanostructures is sensitive to the amount of electromagnetic field probing the active material [25–27], we find that the analysis of the Faraday effect in these perforate membranes provides a further insight into the origin of the extraordinary transmission.

The rest of the manuscript is organized as follows. First, in section 2 we describe the system under study and we briefly explain the methodology employed to analyze the Faraday effect in this system. Section 3 is devoted to a detailed discussion of the results where we present a systematic study of the system parameters that optimize the performance of our hybrid perforated membranes as Faraday rotators, i.e., we search for the best trade-off between high transmittance and high Faraday rotation. The main conclusions of our work are summarized in section 4. Finally, we show the Faraday rotation and ellipticity of our system in appendix A; in appendix B

we briefly explain how the dispersion relations of the SPPs mentioned in section 3 were actually calculated; whereas appendix C is devoted to the comparison of the electromagnetic field inside a Au membrane at a resonance wavelength and out-of-resonance.

2. Hybrid perforated membranes and Faraday effect

The system that we investigate in this work consists of a hybrid Au-Co-Au perforated membrane featuring a periodic array of sub-wavelength holes forming a square lattice, see Fig. 1(a). The Co layer, which is sandwiched between the two Au layers, has a thickness of t_{Co} and it is located at a distance d from the upper part of the membrane, see Fig. 1(b). Unless otherwise stated, we assume that the substrate is made of glass with a refraction index of 1.5 in the whole visible range and the incident medium is air. For the sake of concreteness, the lattice parameter of the hole array is 400 nm, the hole diameter is 228.6 nm (lattice parameter/1.75), and the total thickness of the membrane is 250 nm. These numbers were inspired by the experiments of [28] where the optical transmission was investigated in perforated membranes of several noble and transition metals. Let us emphasize that with this choice for the geometrical parameters of the system, the optical transmission through these membranes is dominated by the extraordinary optical transmission.
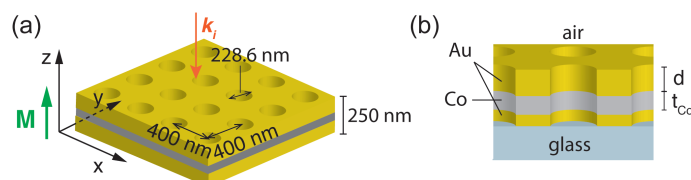

Fig. 1. (a) Schematic representation of the system under study where one can see the Au-Co-Au perforated membrane with a periodic array of holes forming a square lattice. We specify the values of different geometrical parameters such as the lattice constant, the hole diameter, and the membrane total thickness. We also indicate that in the Faraday configuration the Co magnetization, M, is perpendicular to the plane of the membrane and parallel to the light propagation. (b) Lateral cut of the hybrid membrane that sits on a glass substrate. We define here the Co thickness, t_{Co}, and the Co depth or distance between the Co layer and the upper part of the membrane, d.

Our main goal is the theoretical analysis of the Faraday effect in these hybrid perforated membranes. Let us remind that this magneto-optical phenomenon consists in the rotation of the polarization plane of the transmitted light (with respect to the incident light) when the magnetization of the sample is parallel to the direction of the light propagation [29]. Moreover, this rotation is accompanied by a change in the ellipticity. In our case, we shall assume that the light has a perpendicular incidence and it is polarized along the x-axis, which coincides with the high symmetry direction of the square lattice, see Fig. 1(a). In this case, the Faraday rotation is given by $\theta = \mathrm{Re}\{t_{yx}/t_{xx}\}$, while the corresponding ellipticity is given by $\eta = \mathrm{Im}\{t_{yx}/t_{xx}\}$. Here, t_{ij} with $i,j = x,y$ are the complex transmission amplitudes of the structure. In this work we focus on the analysis of the magnitude of the polarization conversion, $|t_{yx}|$, since this quantity represents the purely magneto-optical contribution and leads us to a better understanding of the physics behind our system. A representation of the Faraday rotation and ellipticity is left for appendix A. It is also customary to quantify the magneto-optical activity by combining the rotation and ellipticity in the following quantity: $\Phi_F = \sqrt{\theta^2 + \eta^2}$, which we report in degrees. On the other hand, since it is highly desirable that a Faraday rotation be accompanied by a high transmission, to assess the performance of the system as a Faraday rotator it is convenient to define a figure of merit (FoM) as the product of Φ_F and the zero-order transmittance (for

x-polarized light), T, *i.e.*

$$\text{FoM} = \Phi_F T. \tag{1}$$

In order to compute the different transmission amplitudes in these membranes we have made use of a generalization of the scattering-matrix approach of Whittaker and Culshaw [30] that we have recently put forward [31]. This generalization allows us to describe any magneto-optical effect in periodically patterned multilayer structures. It is worth stressing that in this approach we make use of the so-called fast Fourier factorization, see appendix A of [31], which allows us to solve the traditional convergence problems of scattering approaches when dealing with metallic periodic systems. In this sense, let us remark that all the quantities shown in this work were converged to an accuracy of better than 1% (relative error). Finally, let us say that the optical constant of Au were taken from [32], while the optical and magneto-optical constants of Co were taken from [33].

3. Results

In this section we present a detailed study of the Faraday effect in our Au-Co-Au perforated membranes as a function of both the thickness of the Co layer, t_{Co}, and its position d measured with respect to the upper part of the membrane. Let us start analyzing how the amount of Co influences the Faraday rotation and the corresponding figure of merit. In Fig. 2 we show the results for transmittance T, the polarization conversion in the transmitted light $|t_{yx}|$, and the corresponding figure of merit. These quantities are shown as colormap as a function of the wavelength and the thickness of the Co layer. The Co layer is kept in the middle of the structure and its thickness varies from 10 nm to 250 nm (this latter value corresponds to a pure Co system). For completeness, the corresponding Faraday rotation and the ellipticity are shown in Appendix A.

Starting with the results for the transmittance, shown in Fig. 2(a), notice first that for the thinest Co layer ($t_{Co} = 10$ nm), the transmittance exhibits two maxima at wavelengths around $\lambda_1 = 585$ nm and $\lambda_2 = 710$ nm, which are very close to the spectral position of the two maxima observed in pure Au membranes [28]. These maxima are the manifestation of the extraordinary optical transmission and they are reported to originate from the excitation of the SPPs in both Au-dielectric interfaces. To be precise, a simple analysis of the SPPs in these membranes, see Appendix B, points to that the maximum around λ_1 has a mixed character, and is mainly due to the excitation of the SPP in the air-Au interface with a weaker contribution from a second order plasmon formed in the back interface. On the other hand, the transmittance maximum around λ_2 is due to the SPP in the Au-glass interface, see Appendix C. The mixed character of the high frequency maximum will unravel itself along the manuscript. As the Co thickness increases, the transmittance not only decreases, but the maxima are also shifted to smaller wavelengths, reaching values of 460 nm and 660 nm respectively when the film is 100% Co. The reduction of the transmittance is a simple consequence of the larger absorption in Co, as compared to Au (notice that there is also a broadening of the peaks, also consequence of a larger absorption). Paying attention now to the polarization conversion, see Fig. 2(b), the situation is basically reversed, *i.e.* the conversion progressively increases as the amount of Co increases in the structure and the maxima occur approximately at the same wavelength as the maxima in the transmittance of the membrane without Au. Notice, however, that the polarization conversion does not reach a maximum when the Au is entirely removed. This illustrates the fact that the presence of a Au layer next to the incident medium is beneficial for both the transmittance and the magneto-optical properties, which is due to the low-damping SPPs excited in the air-Au interface. Finally, when combining these two properties into the figure of merit to find the best compromise between a large rotation and a good transmittance, see Fig. 2(c), we find that there is no a unique optimal configuration for the whole visible range. Depending on the working
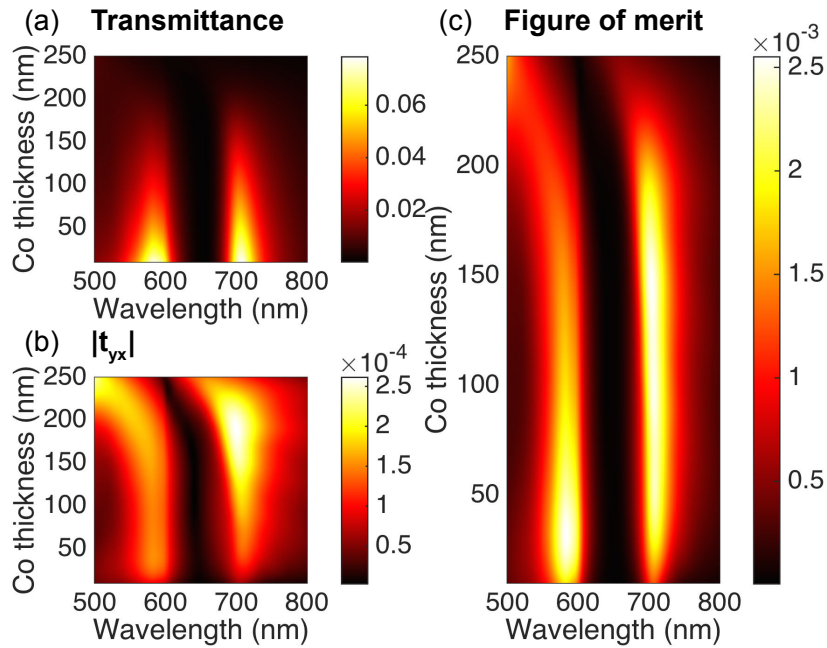
Fig. 2. (a) Transmittance as a function of the wavelength and the thickness of the Co layer, which lies in the middle of the structure. (b) The corresponding magnitude of the coefficient t_{yx} that describes the polarization conversion of the transmitted light. (c) Figure of merit (FoM), as defined in Eq. (1).

range of wavelengths, it would be possible to choose between two different configurations. For smaller wavelengths, an optimal configuration is reached when $t_{Co} \simeq 30$ nm, while for larger wavelengths the choice would be $t_{Co} = 150$ nm. It is worth remarking that in both cases, the figure of merit of these hybrid systems can reach values that are more than one order of magnitude larger than in the case of a pure Co membrane.

Let us now analyze the role of the position of the Co layer, as it has been reported to play an important role in both continuous films [25, 27] and disks [26]. For this purpose, we have fixed the thickness of the Co layer to $t_{Co} = 10$ nm (this thickness is enough to have a reasonable MO activity while it does not perturb significantly the internal electromagnetic field [26]) and varied its position from $d = 0$ (top of the membrane) to $d = 240$ nm (bottom of the membrane). In Fig. 3 we gather the results for the transmittance, polarization conversion, and figure of merit as a function of both the wavelength and the distance d. The corresponding Faraday rotation and the ellipticity are shown in Appendix A. The first thing to notice is that for all positions of the Co layer, there is a maximum for the three quantities around λ_1 and λ_2. However, when the Co is placed close to the top the transmittance around λ_1 exhibits a broadened, damped maximum, while the one around λ_2 is more intense and sharper. Conversely, the polarization conversion and the figure of merit exhibit a maximum more intense and broader around λ_1. This is a clear indication of the influence of the Co on the plasmon at the top interface, with a larger influence on the polarization conversion and broadening of the features. The situation is reversed when the Co layer is placed close to the bottom, the transmittance peak around λ_2 appears damped and broadened, whereas the polarization conversion and figure of merit reaches its maximum. However, the features at λ_1 also experiment modifications, such as a weak damping and blue shift of the transmission peak, as well as a pronounced enhancement of the figure of merit and
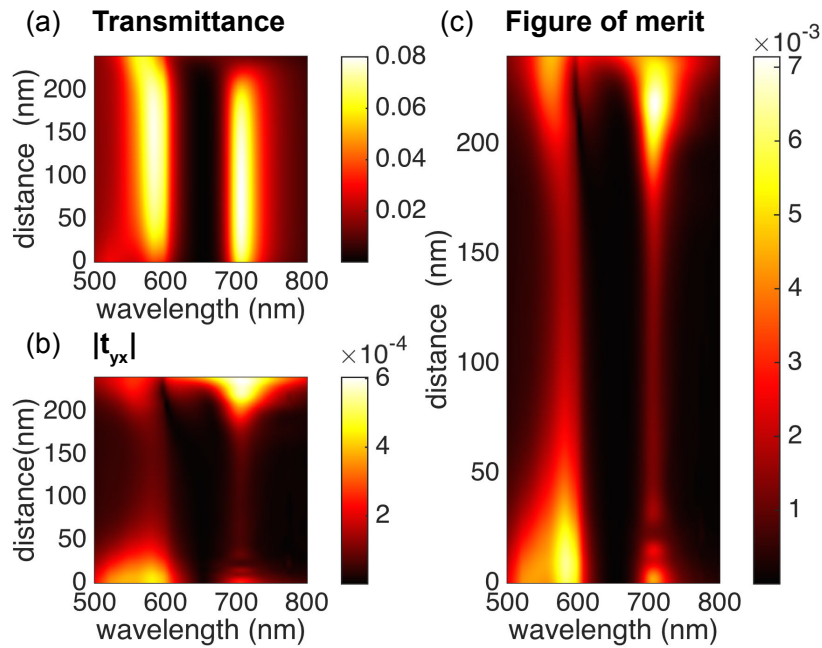
Fig. 3. (a) Transmittance as a function of the wavelength and the position of a 10 nm-thick Co layer, measured with respect to the upper part of the hybrid membrane. (b) The corresponding value of the polarization conversion $|t_{yx}|$ and (c) figure of merit.

polarization conversion. This reflects the fact that there is an influence of a plasmon excitation at the back side, pointing to the aforementioned mixed character of the mode occurring at λ_1.

In this case, as one can see in Fig. 3(c), the best compromise between reasonable transmission and large Faraday rotation for wavelengths around λ_1 is found when the Co layer is close to the top, but not right at the top, to avoid the large damping due to the high absorption of Co. For wavelengths close to λ_2, it is best to place the Co close to the bottom, but, for the same reason, not at the very bottom. These results for the figure of merit are easy to interpret and, in turn, they provide a very useful insight into the origin of the underlying extraordinary optical transmission. It is obvious that the maximum in the figure of merit close to λ_1 that appears at $d \approx 10$ nm is due to the resonant excitation of the SPP at the air-Au interface. Similarly, the maximum of the figure of merit around λ_2 appears at $d \approx 220$ nm because of the excitation of the corresponding SPP at the Au-glass interface. As we illustrate in appendix C, surface plasmon excitation enhances the electromagnetic field at the interfaces and, therefore, placing the Co layer close to the surface where the plasmon is excited we get an amplification of the electromagnetic field inside the ferromagnetic layer, which leads to an increase in the magneto-optical activity. The mixed character of the SPP around λ_1 is manifested by the peak for d close to the membrane-substrate interface. The larger absorption in Co makes it disadvantageous to place the layer of this material right at the top or bottom of the membrane.

So far, we have kept fixed the index of refraction of the incidence and the substrate media. In what follows, we show that the polarization conversion, and the corresponding figure of merit, can be further tuned (both in magnitude and in wavelength) by playing with the dielectric material both in the medium of incidence and in the substrate. In Fig. 4 we show the same information as in the previous figures, but now as a function of the wavelength and of the index of refraction of the medium of incidence, n_{inc}. In this case, we have fixed the index of refraction

(a) Transmittance

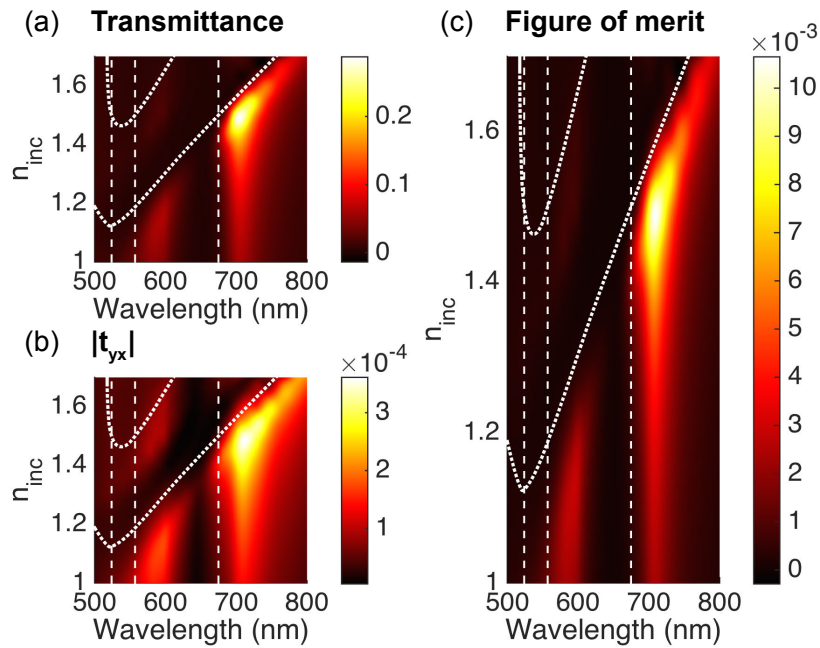**(c) Figure of merit**

(b) |t_yx|

Fig. 4. (a) Transmittance as a function of the wavelength and the index of refraction of the medium of incidence. The index of refraction of the substrate is 1.5. The Co layer has a thickness of 50 nm and it is placed in the middle of the membrane. (b) The corresponding value of $|t_{yx}|$ and (c) figure of merit. In all the panels, the short-dashed lines correspond to the position of the SPPs of the interface between the incidence medium and the upper Au layer, while the vertical long-dashed lines indicate the position of the SPPs in the interface between the lower Au layer and the substrate.

of the substrate to $n_{subs} = 1.5$ and the Co layer has a thickness of 50 nm and it is placed in the center of the membrane, *i.e.* $d = 100$ nm. For single metal membranes, it has been established, both experimentally and theoretically, that the transmittance of a perforated membrane is maximized when the incidence medium and the substrate are made of the same material [34]. The results of Fig. 4 not only confirm this idea, but they also show that the polarization conversion and the figure of merit reach a maximum in the symmetric situation $n_{inc} = n_{subs}$. In this symmetric case the SPPs of the upper and lower interface are excited at the same wavelength and the maxima in the different quantities appear at λ_2. It is worth noticing that when the index of refraction of the incidence medium is 1.5 there is a peak at λ_1, albeit much less intense than that at λ_2. This points to the appearance of a second SPP at λ_1 for $n_{inc} = 1.5$, explaining the mixed character of the SPP at λ_1. To give further insight of the mentioned effect we plot in Fig. 4 the position of a continuous-film SPP with parameters equivalent to those of the upper interface (short-dashed lines) and its evolution as the refraction index of the incidence medium is varied, exhibiting maxima where there is an intersection with a continuous-film SPP with parameters equivalent to those of the substrate (long-dashed lines). These SPP positions were calculated as explained in appendix B, and should be noticed that the approximation is far from accurate for small wavelengths, since the size of the hole becomes more similar to that of the wavelength of the incident light.

Similarly, the same quantities can be tuned by changing the index of refraction of the substrate, n_{subs}. This is shown in Fig. 5 where we display the three quantities as a function of the
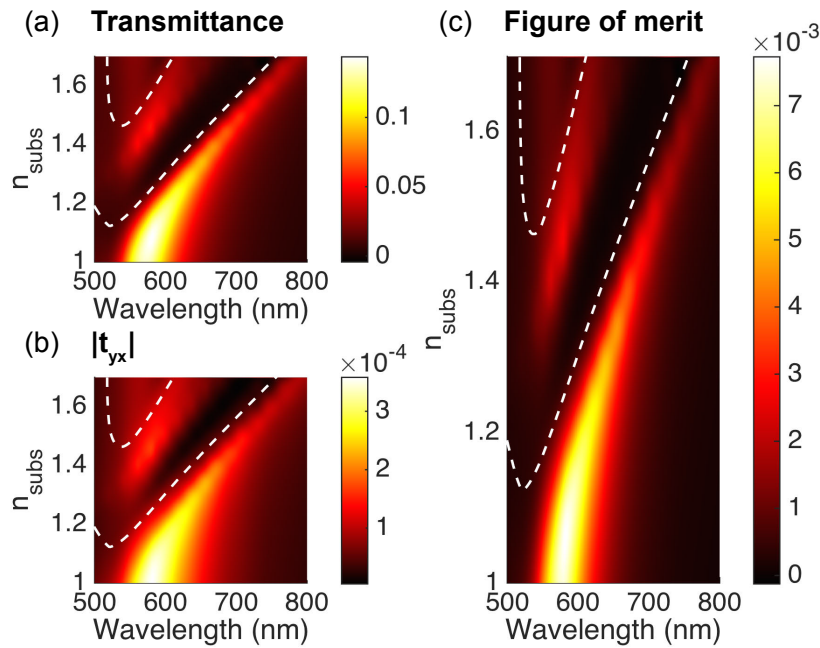
Fig. 5. (a) Transmittance as a function of the wavelength and the index of refraction of the substrate. The index of refraction of the incident medium is 1.5. The Co layer has a thickness of 50 nm and it is placed in the middle of the membrane. (b) The corresponding value of $|t_{yx}|$ and (c) figure of merit. In all the panels, the dashed lines correspond to the position of the SPPs of the interface between the lower Au layer and the substrate.

wavelength and n_{subs}. In this case, we have fixed n_{inc} to 1 and use the same geometrical parameters of the membrane as in Fig. 4. As it can be seen, in Fig. 5, the transmittance, the polarization conversion, and the figure of merit are again maximal in the symmetric case $n_{\text{inc}} = n_{\text{subs}}$. Obviously, this time the maximum in the different quantities appears at λ_1, when the wavelength of the SPP of the upper and lower interfaces when the refraction index is equal to 1. Notice also that at a given value of n_{subs}, the maximum of the three quantities appears at the position of the SPP of the lower interface, and a second SPP appears, being close to λ_1 for $n_{\text{subs}} = 1.5$.

4. Conclusions

We have shown that the Faraday polarization conversion in a magneto-plasmonic crystal made of a perforated membrane with a period array of sub-wavelength holes can be greatly enhanced by combining ferromagnetic and noble metals. This enhancement originates from the phenomenon of the extraordinary optical transmission, which in turn stems from the resonant excitation of SPPs at the interfaces of these perforated membranes. We have illustrated this idea with a systematic analysis of the Faraday effect in a hybrid Au-Co-Au perforated membrane. We have shown that the performance of these metallic membranes as Faraday rotators can be maximized, for a certain wavelength range, by placing the Co layer close to the upper or lower interfaces, but not right at the edge. In both cases, the enhanced performance is due to the excitation of the SPPs in the outer Au layer. This excitation leads to an enhancement of the electromagnetic field in the Co layer, which in turn is reflected as an increase in the magneto-optical signal (the polarization conversion). Moreover, we have shown that the analysis of the magneto-optical activity of these perforated membranes provides a new insight

into the extraordinary optical transmission. Finally, we can anticipate that the combination of ferromagnetic and noble metals in the context of perforated membranes with periodic arrays of sub-wavelength holes may lead to a dramatic enhancement of a variety of magneto-optical phenomena.

Appendix A: Faraday rotation and ellipticity

Throughout the manuscript we have evaluated the performance of our perforated membranes in terms of the figure of merit, FoM, and the polarization conversion, $|t_{yx}|$. For completeness, we report in this appendix the Faraday rotation, $\theta = \mathrm{Re}\{t_{yx}/t_{xx}\}$, and ellipticity, $\eta = \mathrm{Im}\{t_{yx}/t_{xx}\}$, of our Au-Co-Au membranes for the first two issues discussed in the main manuscript. Fig. 6 illustrates the Faraday rotation and ellipticity corresponding to the first issue where we place a Co layer in the middle and vary its thickness from 10 nm to 250 nm. As one can see, the maximum Faraday rotation takes place at around 700 nm and when the structure does not contain almost any Au. This seems to suggest that it is deleterious to include Au in the structure. However, this impression is wrong since the maximum of the Faraday rotation is accompanied by a vanishing transmission, see Fig. 2(a), which is obviously not desirable. This fact nicely illustrates why it is much more convenient in our case to gauge the performance of the device in terms of the figure of merit introduced in this work. Finally, we display in Fig. 7 the Faraday rotation and ellipticity of our system with a 10 nm-thick Co layer as a function of its distance from surface, which correspond to the results shown in Fig. 3.
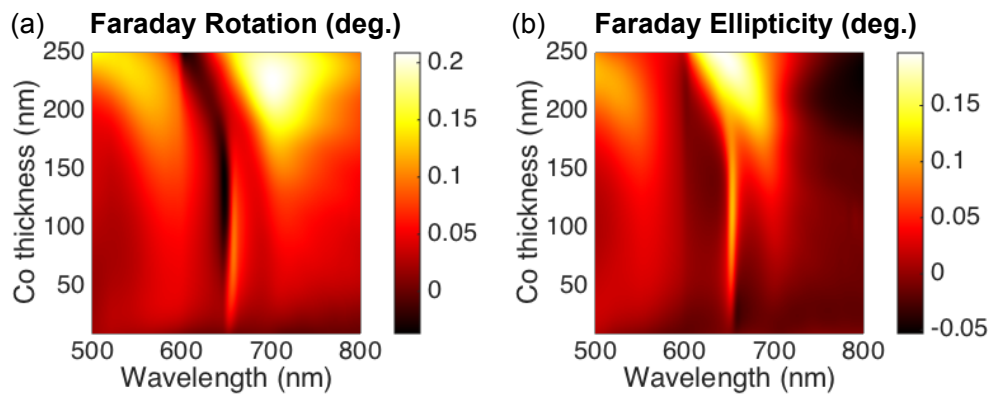

Fig. 6. (a) Faraday rotation and (b) Faraday ellipticity as a function of the wavelength and the thickness of the Co layer, which lies in the middle of the structure. The results correspond to those of Fig. 2.

Appendix B: Bragg surface plasmon polaritons

In this appendix we shall briefly explain how the dispersion relation of the SPPs included in section 3 were calculated. All the SPPs alluded in that section referred to the Bragg plasmons of a single interface between a metal and a dielectric. To determine the position of those plasmon modes, we used the following approximation. First, we consider the dispersion relation for the continuous films, which is given by [35]

$$k_{\mathrm{spp}}(\lambda) = \frac{2\pi}{\lambda}\sqrt{\frac{\varepsilon_{\mathrm{m}}(\lambda)\varepsilon_{\mathrm{d}}}{\varepsilon_{\mathrm{m}}(\lambda) + \varepsilon_{\mathrm{d}}}}, \tag{2}$$

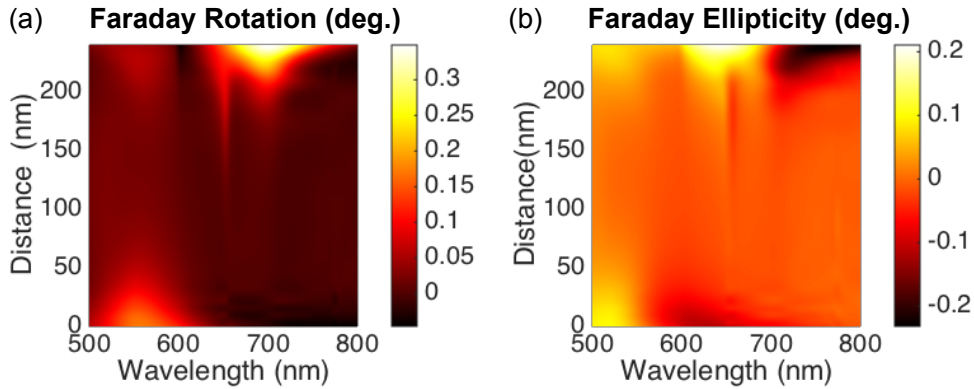**(a)** **Faraday Rotation (deg.)**   **(b)** **Faraday Ellipticity (deg.)**

Fig. 7. (a) Faraday rotation and (b) Faraday ellipticity as a function of the wavelength and the position of a 10 nm-thick Co layer, measured with respect to the upper part of the hybrid membrane. The results correspond to those of Fig. 3.

where k_{spp} is the complex wave vector of the SPP, λ is the light wavelength, and $\varepsilon_{\text{m}}(\lambda)$ and ε_{d} are the dielectric constants of the metal and the dielectric, respectively. For the metal case $\varepsilon_{\text{m}}(\lambda)$ we have simply considered it to be a geometrical average of $\varepsilon_{\text{Au}}(\lambda)$ and $\varepsilon_{\text{air}} = 1$. Now, for perpendicular incidence, the matching condition for the excitation of the SPPs, which is the conservation of the parallel wave vector, can be written as

$$|\text{Re}\left\{k_{\text{spp}}(\lambda_{n_1,n_2})\right\}| = |\mathbf{G}_{n_1,n_2}|, \tag{3}$$

where $\mathbf{G}_{n_1 n_2}$ is a reciprocal lattice vector of the square lattice. The condition of Eq. (3) tells us at which (discrete) wavelengths can couple to the SPPs considering normal incidence. The different dispersion relations or positions of the SPPs mentioned and shown in section 3 were calculated by solving numerically Eq. (3).

Appendix C: Electric field inside the Au membrane

In order to illustrate the excitation of the surface plasmon at the substrate interface, in this appendix we present the distribution of the electric field inside a Au membrane at two different wavelengths, one corresponding to the surface plasmon resonance, Fig. 8(a) and Fig. 8(b), and one out-of-resonance wavelength, Fig. 8(c) and Fig. 8(d). The Au membrane used on this appendix has the same dimensions as those used throughout the manuscript, i.e., a lattice parameter of 400 nm and a hole diameter of 228.6 nm. First, let us compare the distributions of the electric field in a cross-section (*xz*-plane at $y = 0$) of the Au membrane corresponding to the resonance and out-of-resonance wavelengths, Fig. 8(a) and Fig. 8(c), respectively. We can unmistakably see an enhancement of the electric field inside the lower part of the hole at the wavelength where a plasmon excitation takes place. This situation is in accordance with the phenomenon of the extraordinary optical transmission reported for that concrete wavelength [28]. Moreover, we see that the electric field at the base of our membrane - substrate interface - is enhanced compared to the field at the wavelength where we do not expect to have any plasmon resonance. To see this fact more clearly, we have depicted the magnitude of mean value of the electric field inside the metallic part of the membrane along the *z*-axis, Fig. 8(b) and Fig. 8(d). In Fig. 8(b) we observe a noticeable enhancement of the electric field close to the substrate ($z = 0$), which corroborates a surface plasmon polariton excitation at $\lambda = 710$ nm.
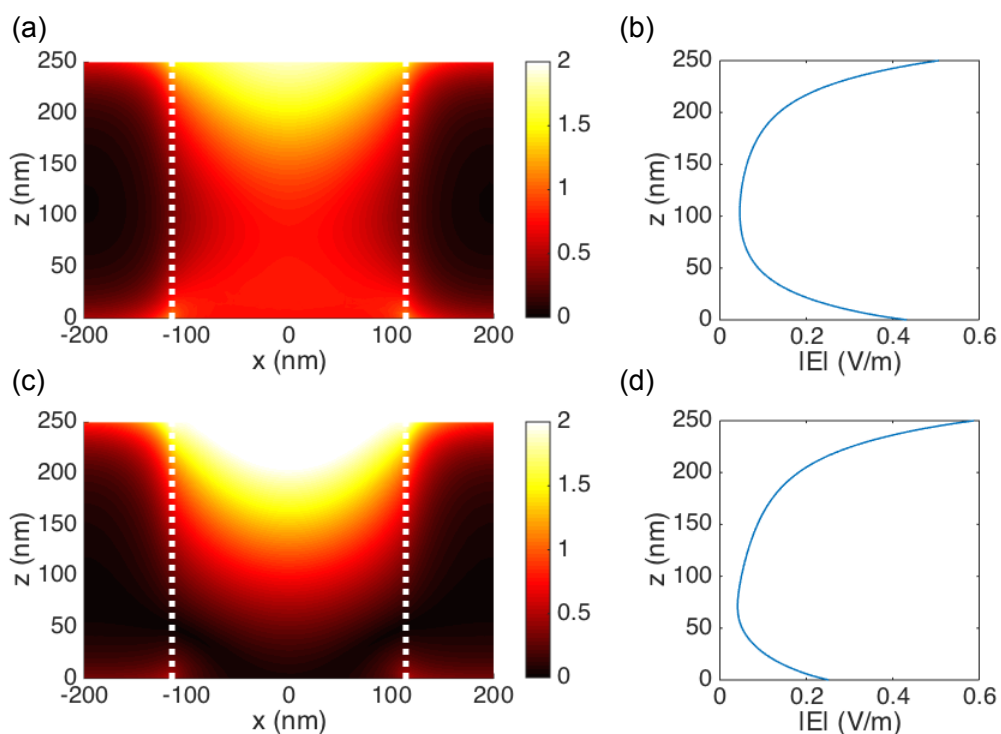
Fig. 8. (a) and (c) Cross section of the electric field distribution in the Au membrane at the resonance wavelength ($\lambda = 710$ nm) and out-of-resonance ($\lambda = 655$ nm), respectively. White dotted line represents the hole boundaries. (b) and (d) Mean value of the electric field in the Au membrane along the z-axis for $\lambda = 710$ nm and $\lambda = 655$ nm, respectively.